Uptake Mechanisms and Regulatory Responses to MECAM- and DOTAM-Based Artificial Siderophores and Their Antibiotic Conjugates in Pseudomonas aeruginosa

Sarah Fritsch, Véronique Gasser, Carsten Peukert, Lukas Pinkert, Lauriane Kuhn, Quentin Perraud, Vincent Normant, Mark Brönstrup, Isabelle Schalk

Uptake mechanisms and regulatory responses to MECAM- and DOTAM-based artificial siderophores and their antibiotic conjugates in *Pseudomonas aeruginosa*

Journal:	*ACS Infectious Diseases*
Manuscript ID	id-2022-00049q.R1
Manuscript Type:	Article
Date Submitted by the Author:	n/a
Complete List of Authors:	Fritsch, Sarah; University of strasbourg, UMR7242 Gasser, Véronique; Université de Strasbourg-CNRS, UMR 7242, Biotechnologie et Signalisation Cellulaire Peukert, Carsten; Helmholtz Centre for Infection Research, Department of Chemical Biology Pinkert, Lukas; Helmholtz Centre for Infection Research, Department of Chemical Biology Kuhn, Lauriane; Institut de Biologie Moléculaire et Cellulaire, Plateforme Proteomique Strasbourg - Esplanade Perraud, Quentin; University of Strasbourg Normant, Vincent; Université de Strasbourg, Brönstrup, Mark; Helmholtz-Zentrum fur Infektionsforschung GmbH, Chemical Biology Schalk, Isabelle; University of Strasbourg - CNRS, UMR7242

Uptake mechanisms and regulatory responses to MECAM- and DOTAM-based artificial siderophores and their antibiotic conjugates in *Pseudomonas aeruginosa*

Sarah Fritsch[1,2], Véronique Gasser[1,2], Carsten Peukert[4], Lukas Pinkert[4], Lauriane Kuhn[3], Quentin Perraud[1,2], , Vincent Normant[1,2], Mark Brönstrup[4,5,6*] and Isabelle J. Schalk[1,2 *].

[1] CNRS, University of Strasbourg, UMR7242, UMR7242, ESBS, Bld Sébastien Brant, F-67412 Illkirch, Strasbourg, France

[2] University of Strasbourg, UMR7242, ESBS, Bld Sébastien Brant, F-67412 Illkirch, Strasbourg, France

[3] Plateforme Proteomique Strasbourg - Esplanade, Institut de Biologie Moléculaire et Cellulaire, CNRS, FR1589, 15 rue Descartes, F-67084 Strasbourg Cedex, France

[4] Department of Chemical Biology Helmholtz Centre for Infection Research, Inhoffenstrasse 7, 38124 Braunschweig (Germany)

[5] German Center for Infection Research (DZIF), Site Hannover-Braunschweig, Germany

[6] Center of Biomolecular Drug Research (BMWZ), Leibniz Universität, 30159 Hannover, Germany

[*] Lead contact or to whom correspondence should be addressed: isabelle.schalk@unistra.fr ; mark.broenstrup@helmholtz-hzi.de

Keywords: Antibiotic vectorization, Trojan horse, *Pseudomonas aeruginosa*, siderophores, iron uptake, outer membrane transporters

ABSTRACT

The development of new antibiotics against Gram-negative bacteria has to deal with the low permeability of the outer membrane. This obstacle can be overcome by utilizing siderophore-dependent iron uptake pathways as entrance routes for antibiotic uptake. Iron-chelating siderophores are actively imported by bacteria, and their conjugation to antibiotics allows smuggling the latter into bacterial cells. Synthetic siderophore mimetics based on MECAM (1,3,5-N,N',N"-tris-(2,3-dihydroxybenzoyl)-triaminomethylbenzene) and DOTAM (1,4,7,10-Tetrakis(carbamoylmethyl)-1,4,7,10-tetraazacyclododecane) cores, both chelating iron *via* catechol groups, have been recently applied as versatile carriers of functional cargo. In the present study, we show that MECAM and the MECAM-ampicillin conjugate **3** transport iron into *Pseudomonas aeruginosa* cells *via* the catechol-type outer membrane transporters PfeA and PirA, and DOTAM solely *via* PirA. Differential proteomics and qRT-PCR showed that MECAM import induced the expression of *pfeA*, whereas **3** led to an increase in the expression of *pfeA* and *ampc,* a gene conferring ampicillin resistance. The presence of DOTAM did not induce the expression of *pirA*, but upregulated the expression of two zinc transporters (*cntO* and *PA0781*), pointing out that bacteria become zinc starved in the presence of this compound. Iron uptake experiments with radioactive ^{55}Fe demonstrated that import of this nutrient by MECAM and DOTAM was as efficient as with the natural prototype siderophore enterobactin. The study provides a functional validation for DOTAM- and MECAM-based artificial siderophore mimetics as vehicles for the delivery of cargo into Gram-negative bacteria.

There is an urgent need to find new antibiotics to counter bacterial antibiotic resistance and the situation is particularly alarming for Gram-negative bacteria. The challenge associated with Gram-negative bacteria is the presence of an additional, outer membrane that reduces drug penetration compared to Gram-positive bacteria. Nutrient import pathways involving TonB-dependent transporters (TBDT) are promising entrance routes to deliver antibiotic drugs into Gram-negative bacteria. These TBDTs are embedded in the outer membrane and have a β-barrel structure with a lumen that is closed by the N-terminal region of the transporter forming a plug.[1] The substrate binding site is usually specific for a family of structurally related compounds. Uptake of the substrate depends on the proton motive force, that is transmitted by coupling the TBDT with the TonB protein anchored in the inner membrane in complex with two other inner membrane proteins ExbB and ExbD.[2–6]

TBDTs are involved in the import of essential nutrients as vitamin B12, oligosaccharides and biological metals, but have been mostly investigated for their ability to import ferric iron *via* siderophores.[1,7–11] Ferric iron (the iron form present in aerobic conditions) is poorly soluble in aqueous solutions and poorly bioavailable in the host during infections, because it is mainly protein-bound. To increase access to ferric iron, bacteria produce and secrete siderophores who serve to sequester iron from the environment and transport it back into bacteria *via* TBDTs.[12] Siderophores are small molecules and are usually classified in four groups according to the nature of the dentates used to chelate the ferric iron: hydroxamates (such as ferrioxamine B or ferrichrome), catecholate (enterobactin), carboxylate (rhizobactin) and mixed siderophores (pyoverdine).[12,13] Siderophore are also characterized by a strong affinity for iron, which, in the case of enterobactin (ENT), can reach values up to 10^{42} M^{-1}.[14,15] Often the bacteria produce their own siderophores, but can as well use siderophores produced by other microorganisms in a piracy strategy.[16–18] The opportunist pathogen *P. aeruginosa* produces the two endogenous siderophores pyoverdine (PVD) and pyocheline (PCH)[19], while many chelators from other pathogens can be hijacked as so-called xenosiderophores (Table S1). For each of these siderophores or xenosiderophores, *P. aeruginosa* expresses a specific TBDT and other proteins allowing the dissociation of iron from the chelator.[17,18,20,21] These iron uptake pathways are generally expressed at

very low levels, and bacteria only induce the expression of the most efficient pathway(s) for iron acquisition, depending on the iron sources present.[10] Under iron-restricted conditions, *P. aeruginosa* detects the presence of xenosiderophores in its environment using sigma and anti-sigma factors, two component systems, and transcriptional regulators of the AraC family (Table S1).[10,12–14] In the presence of ferri-xenosiderophores, these regulators activate the transcription of the genes encoding the TBDTs recognizing the (xeno-)siderophores as well as genes encoding other proteins involved in the pathway. When the intracellular iron concentration reaches a certain level, the transcriptional regulator Fur represses the transcription of all genes involved in iron import.[11]

Numerous studies show that these iron import pathways can be used to smuggle antibiotics into bacteria through a 'Trojan Horse' approach.[22–25] If the antibiotic is linked covalently to siderophore units, it is internalized together with the bound ferric iron into the bacterial cell.[22,25–30] The first antibiotic on the market that chelates iron and enters pathogenic cells via the iron uptake pathways is cefiderocol, a cephalosporin-catechol conjugate.[31–33] Siderophores coupled to fluorescent probes or to probes chelating gallium-68 nuclide can also be used to visualize, detect or identify microbial pathogens during infections in animals.[34–38]

The respective TBDTs allowing the accumulation of these antibiotic-siderophore conjugates have not been identified in most cases. The goal of the present work was (i) to evaluate the ability of two siderophore mimetics based on the MECAM (1,3,5-N,N',N"-tris-(2,3-dihydroxybenzoyl)-triaminomethylbenzene) (**1**) and DOTAM (1,4,7,10-Tetrakis(carbamoylmethyl)-1,4,7,10-tetraazacyclododecane) (**4**) scaffolds (Figure 1),[35,39,40] to transport iron and antibiotics into *P. aeruginosa* cells, (ii) to identify the transporters involved, and (iii) to evaluate the modulation of the expression of the different iron uptake pathways of *P. aeruginosa* in the presence of these vectors and their corresponding antibiotic conjugates. MECAM **1** is an analogue of ENT, a tris-catechol-like siderophore produced by *E. coli* that is used as a xenosiderophore by *P. aeruginosa*.[4,17,41,42] We also examined the MECAM-ampicillin conjugate **3**, which has a minimal inhibitory concentration lower than 90 nM on *E. coli* and *A. baumannii* growth and no activity on *P. aeruginosa*.[40] Ampicillin is usually

inactive on *P. aeruginosa* strains due to the low permeability of the outer membrane and its ability to induce the expression of the β-lactamase AmpC.[43] The DOTAM-based siderophore **4** is a bifunctional compound with two separate metal binding sites, one for iron at the catechol units and a second one at the cyclen.[35] This vector has been linked either to an antibiotic (daptomycin; compound **6**) or to a DOTA unit commonly used for a radionuclide chelation (compound **7**). Conjugate **7** was found to be suitable for positron emission tomography (PET) imaging and was able to discern *E. coli* infection from a lipopolysaccharide-triggered, sterile inflammation.[39] For both vectors, MECAM and DOTAM, the deacetylated and acetylated forms were tested, as the acetylated forms avoid *in vivo* deactivation of the iron chelating units by catechol-*O*-methyltransferases.[44] Because the antibiotic conjugates had no antimicrobial activity on *P. aeruginosa* (Table S2), they were used here as tools to study uptake mechanisms and responses.

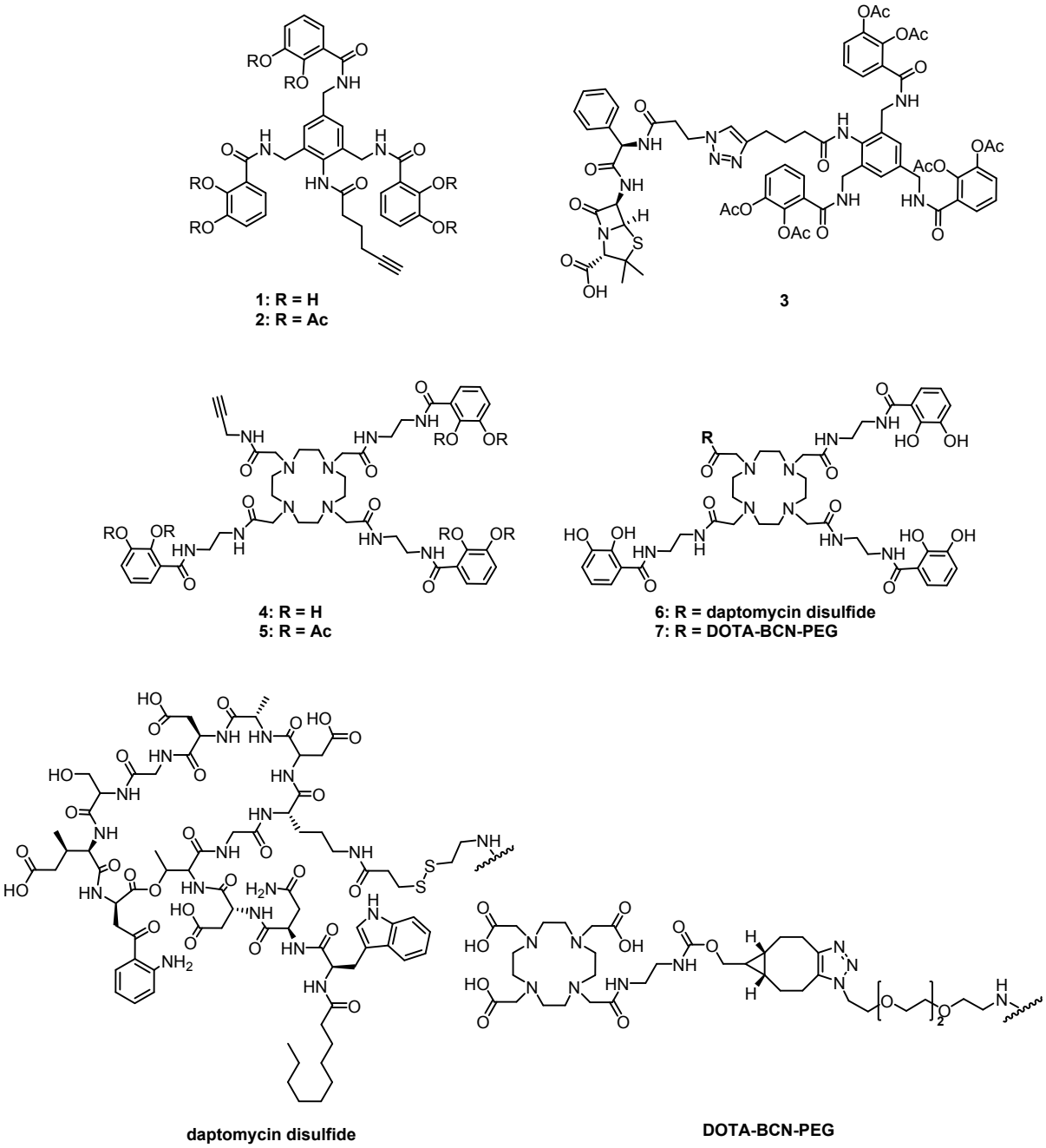

Figure 1: Structures of MECAM (1/2), DOTAM (4/5) and the conjugates 3, 6 and 7.

RESULTS

MECAM- and DOTAM-based artificial siderophores compete for ferric iron with PVD. In order to investigate whether MECAM and DOTAM could compete for iron with *P. aeruginosa's* endogeneous siderophores PVD and PCH, a fluorescence assay was applied. PVD, which has a higher affinity for ferric

iron than PCH (K_a of $10^{30.8}$ M^{-1} for PVD vs 10^{18} M^{-2} for PCH), emits fluorescence at 447 nm in its apo form upon excitation at 400 nm (pH 7.0), whereas the PVD-Fe complex is non-fluorescent.[45–47]

Non-fluorescent PVD-Fe (10 µM) was incubated with increasing concentrations of MECAM (**1**), DOTAM (**4**), the corresponding conjugates, and the positive control siderophores ENT and ferrichrome (FERRI)[17] (Figure 2). A complete removal of ferric iron from PVD was only observed for ENT at concentrations of approximately 20 µM. As previously described, ferrichrome was unable to completely remove iron from PVD at the tested concentrations.[17] These results are consistent with the siderophore's affinity for iron: K_a of 10^{49} M^{-1} for ENT[15], 10^{29} M^{-1} for ferrichrome[48], and $10^{30.8}$ M^{-1} for PVD.[45] The normalized fluorescence values of **1** and **4** indicate that these two siderophores exhibited a similar efficiency in removing iron from PVD, but they were less efficient than FERRI or ENT at a single timepoint of 48h (Figure 2A). The linkage of an antibiotic moiety to either of the siderophore, conjugates **3**, **6** or **7** did not significantly affect their iron chelation properties (Figures 2B and 2C).

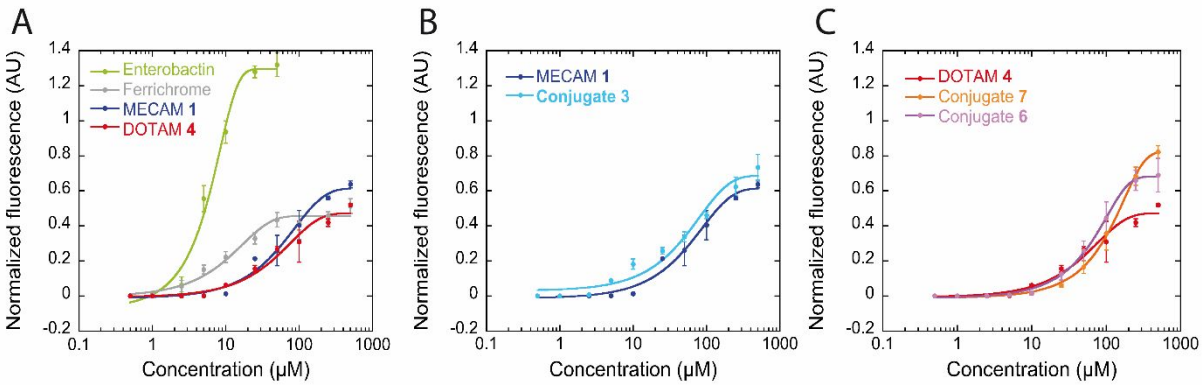

Figure 2: Iron scavenging from PVD-Fe by MECAM- and DOTAM-based siderophores. PVD-Fe at 10 µM was incubated with increasing concentrations of siderophores or conjugates for 48 h in 100 mM HEPES pH 7.4. Apo PVD formation was followed by monitoring its fluorescence at 447 nm (excitation at 400 nm). The experiment was carried out under exactly the same conditions with ENT and ferrichrome (panel A), to compare their iron scavenging properties with those of compounds **1**, **3** (panel B), **4**, **6** and **7** (panel C). Standard deviations were calculated from three independent experiments.

MECAMs 1-3 induce changes in expression of iron uptake-associated proteins in *P. aeruginosa*. Because MECAM-ampicillin **3** showed no antibiotic effect on *P. aeruginosa* cells, the compound was suited as a tool to investigate the phenotypic adaptation of *P. aeruginosa* to its presence using quantitative proteomics. *P. aeruginosa* adapts the expression of its different iron import pathways according to environmental stimuli such as natural or synthetic siderophores.[17,20,42,49–52]

Cells were grown over 8 h in iron-restricted medium (CAA medium, iron concentration = 20 nM (acc. to our previous work[53]) in the absence or presence of **1-3** and analyzed by differential proteomics (Figure 3 for **1** and **3** and Figure S1 for **2**). The deacetylated and acetylated forms of MECAM (**1**/**2**) strongly induced the expression of the TBDT PfeA. A moderate overexpression of PirA was observed in the case of MECAM **2** (Figure 3C). PfeA and PirA have been described in the literature as the TBDTs for ferric iron uptake by ENT in *P. aeruginosa*.[4,41,42,54] Their transcription is regulated by their corresponding two-component systems, with the sensor PfeS and the transcriptional regulator PfeR for *pfeA* and PirS (sensor) and PirR (transcriptional regulator) for *pirA* (Figure S2).[17,42,55] For example, to induce *pfeA* transcription, ferri-ENT, after its uptake across the outer membrane, interacts in the bacterial periplasm with PfeS, which then releases PfeR to activate *pfeA* transcription. In analogy, an induction of *pfeA* expression in the presence of **1** and **2** provides clear evidence that both compounds were able to cross *P. aeruginosa's* outer membrane to interact with PfeS in the bacterial periplasm. An increased expression of FemA (yersiniabactin TBDT) was also observed in the presence of **1** and **2,** albeit with low statistical significance (Figure 3C and S1C). The presence of **3** also induced the expression of PfeA, but to a lower extent compared to **1** and **2**, whereas PirA expression remained unchanged. In parallel, the expression of proteins involved in ferric iron uptake by PCH was repressed by **1-3** (Figure 3D), whereas proteins associated with the PVD pathway were not affected (Figure 3F). Notably, **3** also led to a strong induction of AmpC (Figure 3E). The protein data for **1** and **3** were confirmed by RT-qPCR for the corresponding genes *pfeA*, *fptA*, *fpvA* and *ampC* (Figure S3).

Overall, **1-3** induced the transcription and expression of the gene encoding PfeA, suggesting that (i) the transporter was able to import the iron-loaded compounds **1-3** into *P. aeruginosa* cells and that

(ii) **1-3** were able to activate the two-component system PfeS/PfeR (Figure S2). This phenotypic adaptation of the iron uptake pathway was accompanied by a repression of genes involved in the PCH-dependent iron uptake pathway, which forced the bacteria to preferentially use **1**-**3** to access extracellular iron. The induction of *ampC* expression suggests that the absence of antibiotic is due to the serine-β-lactamase activity of AmpC, which hydrolysed the β-lactam ring of MECAM-ampicillin **3**.

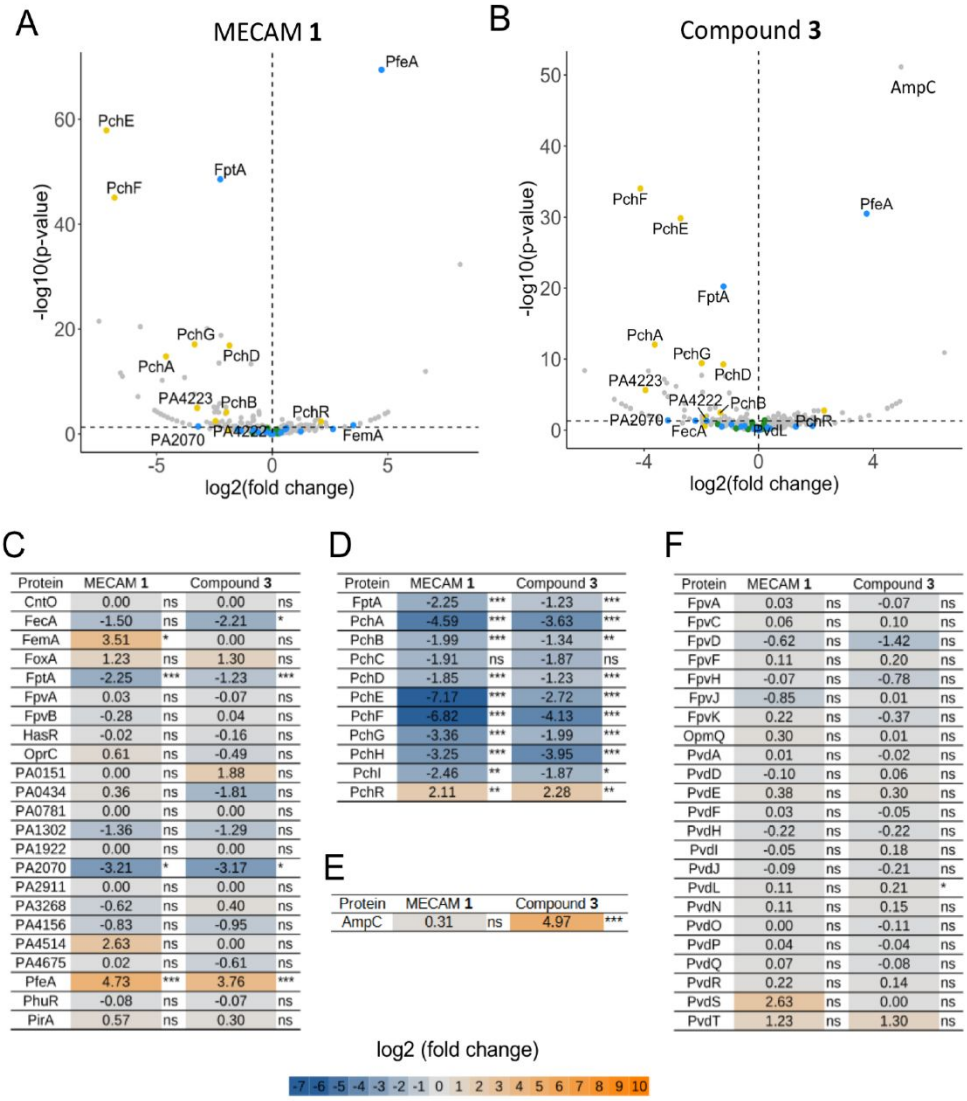

Protein	MECAM 1		Compound 3	
CntO	0.00	ns	0.00	ns
FecA	-1.50	ns	-2.21	*
FemA	3.51	*	0.00	ns
FoxA	1.23	ns	1.30	ns
FptA	-2.25	***	-1.23	***
FpvA	0.03	ns	-0.07	ns
FpvB	-0.28	ns	0.04	ns
HasR	-0.02	ns	-0.16	ns
OprC	0.61	ns	-0.49	ns
PA0151	0.00	ns	1.88	ns
PA0434	0.36	ns	-1.81	ns
PA0781	0.00	ns	0.00	ns
PA1302	-1.36	ns	-1.29	ns
PA1922	0.00	ns	0.00	ns
PA2070	-3.21	*	-3.17	*
PA2911	0.00	ns	0.00	ns
PA3268	-0.62	ns	0.40	ns
PA4156	-0.83	ns	-0.95	ns
PA4514	2.63	ns	0.00	ns
PA4675	0.02	ns	-0.61	ns
PfeA	4.73	***	3.76	***
PhuR	-0.08	ns	-0.07	ns
PirA	0.57	ns	0.30	ns

Protein	MECAM 1		Compound 3	
FptA	-2.25	***	-1.23	***
PchA	-4.59	***	-3.63	***
PchB	-1.99	***	-1.34	**
PchC	-1.91	ns	-1.87	ns
PchD	-1.85	***	-1.23	***
PchE	-7.17	***	-2.72	***
PchF	-6.82	***	-4.13	***
PchG	-3.36	***	-1.99	***
PchH	-3.25	***	-3.95	***
PchI	-2.46	**	-1.87	*
PchR	2.11	**	2.28	**

Protein	MECAM 1		Compound 3	
AmpC	0.31	ns	4.97	***

Protein	MECAM 1		Compound 3	
FpvA	0.03	ns	-0.07	ns
FpvC	0.06	ns	0.10	ns
FpvD	-0.62	ns	-1.42	ns
FpvF	0.11	ns	0.20	ns
FpvH	-0.07	ns	-0.78	ns
FpvJ	-0.85	ns	0.01	ns
FpvK	0.22	ns	-0.37	ns
OpmQ	0.30	ns	0.01	ns
PvdA	0.01	ns	-0.02	ns
PvdD	-0.10	ns	0.06	ns
PvdE	0.38	ns	0.30	ns
PvdF	0.03	ns	-0.05	ns
PvdH	-0.22	ns	-0.22	ns
PvdI	-0.05	ns	0.18	ns
PvdJ	-0.09	ns	-0.21	ns
PvdL	0.11	ns	0.21	*
PvdN	0.11	ns	0.15	ns
PvdO	0.00	ns	-0.11	ns
PvdP	0.04	ns	-0.04	ns
PvdQ	0.07	ns	-0.08	ns
PvdR	0.22	ns	0.14	ns
PvdS	2.63	ns	0.00	ns
PvdT	1.23	ns	1.30	ns

Figure 3: Modulation of protein expression in *P. aeruginosa* in the presence of MECAM 1 and MECAM ampicillin 3. Proteomic analyses were performed on *P. aeruginosa* PAO1 strains grown overnight in CAA medium supplemented with 10 µM **1** (A) or **3** (B). Log2-fold changes in protein abundances and corresponding -log10-transformed p-values relative to untreated control samples are shown in volcano plots. Proteins of the PCH pathway are represented by yellow dots, those of the PVD pathway by green

dots, and the TBDTs by blue dots. C, D, E and F show heat maps of log2-fold changes in TBDT proteins (C), proteins involved in the PCH pathway (D), AmpC protein (E) and proteins of the PVD pathway (F). The darker the shade of blue, the more expression of the protein is repressed; the darker the shade of orange, the more expression of the protein is induced. NS: data not significant; *p < 0.05, **p < 0.01, and ***p < 0.001. Data for **2** are presented in Figure S1.

MECAM 1 and conjugate 3 transport ^{55}Fe into *P. aeruginosa* cells mainly *via* PfeA and to a lower extent via PirA. In order to evaluate the ability of **1** and the corresponding conjugate **3** to transport iron into *P. aeruginosa* cells, the compounds were loaded with radioactive ^{55}Fe and exposed to a Δ*pvdF*Δ*pchA P. aeruginosa* mutant, that is unable to produce the endogenous siderophores PVD and PCH.[51] This mutant was used to avoid any uptake of ^{55}Fe *via* the endogenous siderophores. The experiment was also carried out with *pirA*- and *pfeA*-deficient mutants of Δ*pvdF*Δ*pchA* (Table S3), as these genes encode TBDTs involved in iron acquisition by **1-3** (Figure 3) and by ENT.[42,54,56] Bacteria were grown under iron starvation conditions in order to induce the expression of iron uptake pathways. Both **1** and its corresponding conjugate **3** transported between 250 and 270 pmol ^{55}Fe per $OD_{600\ nm}$ after 1 h incubation, whereas around 200 pmol ^{55}Fe per $OD_{600\ nm}$ were imported in the presence of ENT (Figure 4A). This indicates that **1** and **3** were at least as efficient as the natural siderophore ENT with respect to uptake of iron in *P. aeruginosa* cells. The ^{55}Fe uptake by **1** and **3** was completely abolished in the presence of the protonophore inhibitor carbonyl cyanide m-chlorophenyl hydrazine (CCCP). Because CCCP inhibits any TonB-dependent uptake in bacteria,[57,58] this finding indicates that the uptake of **1** and **3** was not due to passive diffusion *via* porins, but due to an energy-dependent transport relying on TonB. The deletion of the gene *pirA* did not affect ^{55}Fe uptake by **1**, but deletion of *pfeA* resulted in an 80% decrease of ^{55}Fe uptake at 2 h. This indicates that uptake of iron by MECAM occurs essentially *via* PfeA. In the case of **3**, *pfeA* and *pirA* deletions had inhibitory effects of 50% and 22%, respectively. In conclusion, these data show that **1** and **3** were able to transport iron as efficiently as ENT into *P. aeruginosa* cells, with PfeA being the major TBDT involved, while PirA served as a secondary transporter.

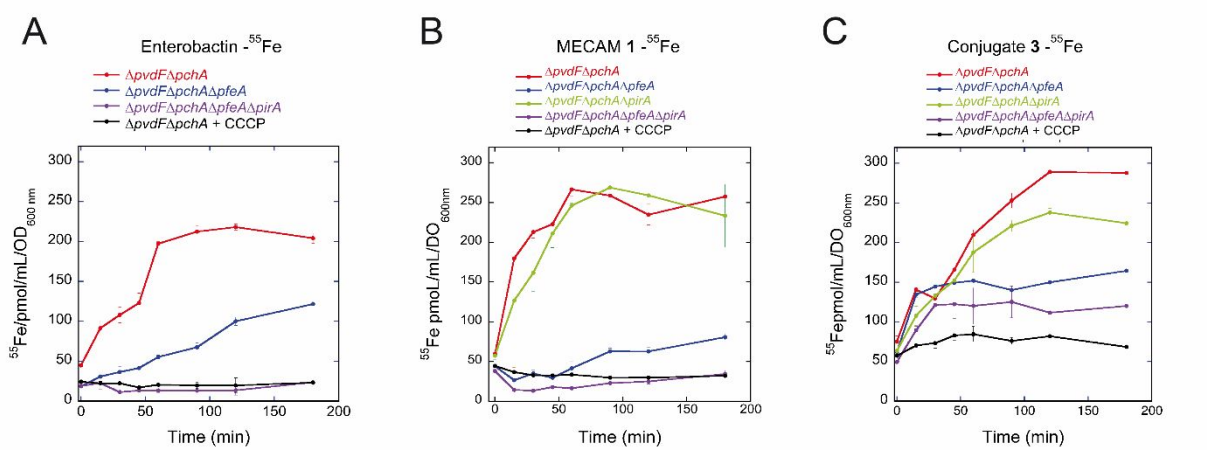

Figure 4: ^{55}Fe uptake in *P. aeruginosa* strains mediated by enterobactin, 1 and 3. *P. aeruginosa* Δ*pvdF*Δ*pchA* and its isogenic Δ*pfeA* and Δ*pirA* mutants, grown in iron-restricted CAA medium and in the presence of 10 µM ENT (A), **1** (B) or **3** (C) to induce the corresponding uptake pathway, were incubated with 500 nM ENT-^{55}Fe (A) , **1**-^{55}Fe (B) or **3**-^{55}Fe (C). The amount of ^{55}Fe taken up into the bacteria was measured as a function of time. As a control, the experiment was repeated in the presence of the protonophore CCCP (200 µM). Errors bars were calculated from three independent biological replicates.

PirA efficiently replaces PfeA in iron uptake via 1 and 3. Next, we sought to determine whether the deletion of *pfeA* or/and *pirA* would have an inhibitory effect on *P. aeruginosa* growth in iron-restricted conditions in the presence of these two compounds. If a given gene deletion leads to a growth inhibition in the presence of the tested siderophore, the knocked-out gene is involved in iron acquisition by the tested siderophore.[58] We used a strain with a Δ*pvdF*Δ*pchA* background that was unable to produce the siderophores PVD and PCH, and the corresponding Δ*pfeA* and Δ*pirA* mutants (Table S3). Δ*pvdF*Δ*pchA* is able to grow in an iron-deficient environment probably using citrate as a siderophore or iron reduction systems with import of ferrous iron through the *feoABC* system.[59–61] Δ*pvdF*Δ*pchA* was grown in CAA medium ± 10 µM of **1** or **3**. The presence of an excess of **1** or **3** chelates all iron traces present in the growth medium making this metal no longer accessible for low affinity import systems. If growth of Δ*pvdF*Δ*pchA* is observed in the presence of **1** or **3**, it demonstrates that the bacteria can access iron *via* these two iron chelators. This is illustrated in Figure S4 with bacillibactin, a catechol type siderophore unable to be used by *P. aeruginosa* cells to import iron: in the presence of 10 µM bacillibactin a strong growth inhibition is observed. Moreover, the presence of

1 or **3**, the single deletion of *pfeA* slightly affected bacterial growth, whereas the single deletion of *pirA* had no effect (Figure 5). In contrast, the deletion of both *pfeA* and *pirA* completely abolished bacterial growth. These results confirm that PfeA is the major TBDT involved in iron acquisition by **1** and **3**. However, if *pfeA* was deleted PirA replaced PfeA efficiently. The same mechanism has been described for iron uptake by ENT, where PirA played a key role only if PfeA was absent.[42]

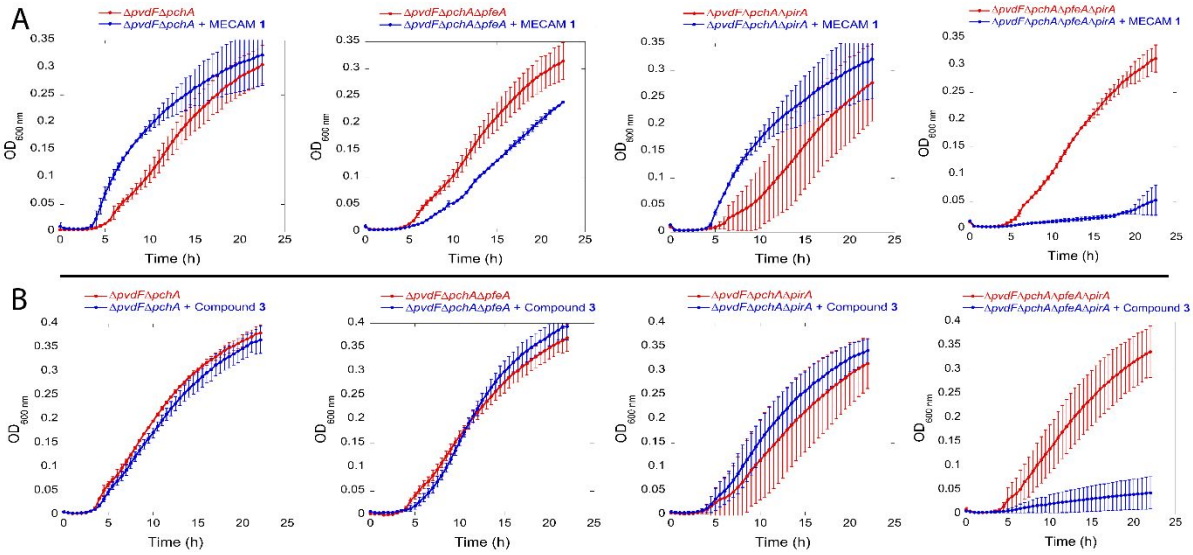

Figure 5. Growth of TBDT-deficient *P. aeruginosa* mutants in the presence of 1 or 3. A PVD and PCH-deficient strain of *P. aeruginosa* (Δ*pvdF*Δ*pchA*) and its corresponding TBDT deletion mutants were used. Strains were grown in CAA medium in the absence (kinetics in red) or presence (kinetics in blue) of 10 µM **1** (A) or **3** (B). Growth was followed by monitoring the optical density (OD) at 600 nm. Errors bars were calculated from three independent biological replicates.

Gene expression modulation in *P. aeruginosa* grown in the presence of DOTAM 4/5 and conjugates 6 and 7. The same proteomic strategy as described above was used to examine genes expression changes in *P. aeruginosa* PAO1 in the presence of the DOTAM-based siderophore **4/5** and the corresponding conjugates **6** and **7** (Figure 6 for compounds **4**, **6** and **7** and Figure S6 for compound **5**). We were surprised to notice that none of the three compounds induced the expression of TBDTs involved in iron uptake to *P. aeruginosa* cells. Instead, the presence of **4**, **5** and **7** increased the expression of CntO and PA0781 (ZnuD), two TBDTs involved in Zn uptake. This was confirmed by RT-

qPCR analysis (Figure S5). CntO imports zinc via the metallophore pseudopaline,[9,62,63] while ZnuD transports zinc ions without the help of any metal chelator.[64,65] These data suggest that **4** and **7** chelated zinc, and bacteria became zinc starved or that **4** and **7** can somehow induce the expression of these two genes via a transcriptional regulator. DOTAM daptomycin **6** did not exhibit this effect. In addition, the expression of proteins of the PCH pathway was repressed by all three compounds. This suggests that less PCH-Fe complexes were formed, probably because **4**, **6** and **7** chelated iron.

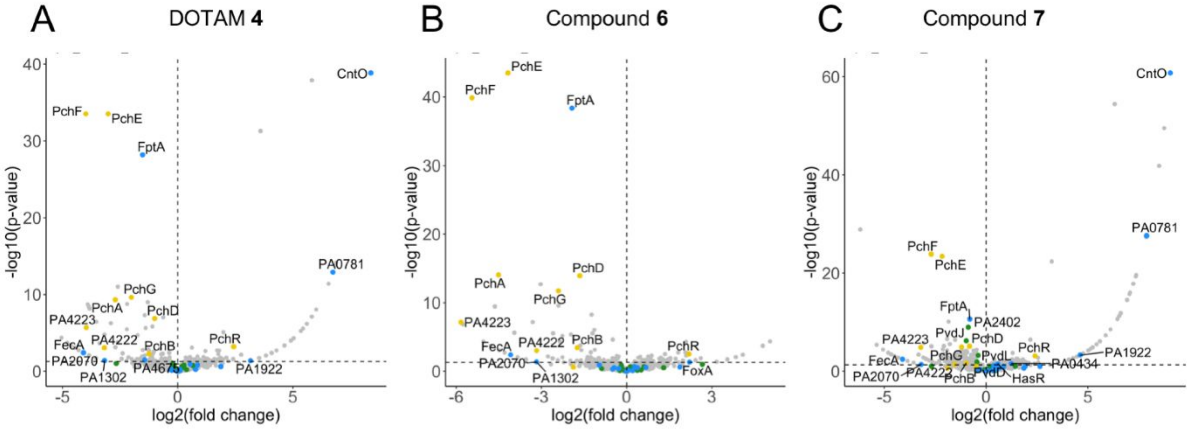

D

Protein	DOTAM 4		Compound 6		Compound 7	
CntO	8.39	***	0.00	ns	9.05	***
FecA	-4.09	**	-4.09	**	-4.11	**
FemA	1.87	ns	1.88	ns	1.86	ns
FoxA	0.78	ns	2.22	*	1.93	ns
FptA	-1.53	***	-1.92	***	-0.80	***
FpvA	0.09	ns	0.06	ns	0.07	ns
FpvB	-0.02	ns	-0.29	ns	-0.29	ns
HasR	0.02	ns	-0.27	ns	0.58	*
OprC	0.55	ns	0.37	ns	0.33	ns
PA0151	1.87	ns	0.00	ns	2.64	ns
PA0434	0.86	ns	0.68	ns	1.24	*
PA0781	6.74	***	0.00	ns	7.89	***
PA1302	-3.18	*	-3.17	*	0.33	ns
PA1922	3.16	*	0.00	ns	4.62	***
PA2070	-3.18	*	-3.17	*	-3.19	*
PA2911	0.00	ns	0.00	ns	1.86	ns
PA3268	-0.26	ns	0.22	ns	0.51	ns
PA4156	0.10	ns	0.01	ns	0.68	ns
PA4514	1.87	ns	0.00	ns	0.00	ns
PA4675	-1.43	*	-0.96	ns	-0.38	ns
PfeA	-0.32	ns	-0.49	ns	0.86	ns
PhuR	0.11	ns	0.28	ns	0.39	ns
PirA	-0.25	ns	-0.44	ns	0.53	ns

E

Protein	DOTAM 4		Compound 6		Compound 7	
FptA	-1.53	***	-1.92	***	-0.80	***
PchA	-2.71	***	-4.51	***	-0.47	ns
PchB	-1.25	**	-1.74	***	-0.98	*
PchC	-0.01	ns	-1.87	ns	-1.89	ns
PchD	-1.00	***	-1.65	***	-0.82	***
PchE	-3.03	***	-4.18	***	-2.16	***
PchF	-3.99	***	-5.44	***	-2.70	***
PchG	-2.01	***	-2.40	***	-1.21	***
PchH	-3.97	***	-5.83	***	-3.21	***
PchI	-3.18	***	-3.17	***	-1.54	*
PchR	2.43	***	2.19	**	2.40	***

log2 (fold change)

-7 -6 -5 -4 -3 -2 -1 0 1 2 3 4 5 6 7 8 9 10

F

Protein	DOTAM 4		Compound 6		Compound 7	
FpvA	0.09	ns	0.06	ns	0.07	ns
FpvC	0.27	ns	0.18	ns	0.47	ns
FpvD	0.38	ns	-0.24	ns	0.35	ns
FpvF	0.27	ns	-0.05	ns	0.29	ns
FpvH	-2.67	ns	0.00	ns	-2.68	ns
FpvJ	-0.01	ns	0.51	ns	0.47	ns
FpvK	-0.01	ns	-0.88	ns	-0.42	ns
OpmQ	-0.01	ns	0.38	ns	1.43	ns
PvdA	0.04	ns	0.07	ns	0.11	ns
PvdD	0.19	ns	0.01	ns	-0.45	*
PvdE	0.66	ns	0.61	ns	0.33	ns
PvdF	0.09	ns	0.09	ns	0.22	ns
PvdH	-0.16	ns	-0.19	ns	-0.08	ns
PvdI	-0.22	ns	0.02	ns	-0.88	***
PvdJ	-0.19	ns	-0.17	ns	-0.98	***
PvdL	0.03	ns	0.12	ns	-0.39	***
PvdN	0.27	ns	0.21	ns	0.20	ns
PvdO	-0.01	ns	-0.05	ns	0.03	ns
PvdP	-0.05	ns	-0.08	ns	0.03	ns
PvdQ	0.01	ns	-0.03	ns	0.01	ns
PvdR	0.18	ns	0.13	ns	0.13	ns
PvdS	0.00	ns	2.67	ns	0.00	ns
PvdT	0.78	ns	1.30	ns	-0.03	ns

Figure 6: Modulation of protein expression in *P. aeruginosa* in the presence of DOTAM-based siderophore 4 and the associated conjugates 6 and 7. Proteomic analyses were performed on *P. aeruginosa* PAO1 strains grown overnight in CAA medium supplemented with 10 µM of DOTAM-based siderophores **4** (A), **6** (B) or **7** (C). Log2-fold changes in protein abundances and corresponding -log10-transformed p-values relative to untreated control samples are shown in volcano plots. Proteins of the PCH pathway are represented by yellow dots, those of the PVD pathway by green dots, and the TBDTs by blue dots. C, D, E and F show heat maps of log2-fold changes in TBDT proteins (C), proteins involved in the PCH pathway (D), AmpC protein (E) and proteins of the PVD pathway (F). The darker the shade of blue, the more expression of the protein is repressed; the darker the shade of orange,

the more expression of the protein is induced. NS: data not significant; *p < 0.05, **p < 0.01, and ***p < 0.001. Data for **5** are presented in Figure S6.

Deletion of *pirA* inhibits bacterial growth in the presence of DOTAM. For the DOTAM-based siderophores **4**, **6** and **7**, ^{55}Fe uptake assays could not be carried out due to micro-precipitation of the compounds and hence significant background noise in the radioactivity signal. In consequence, only the growth assay under iron restricted conditions has been used to test for iron transport of DOTAM and its conjugates into bacteria and to identify the potentially TBDTs involved. Δ*pvdF*Δ*pchA*, the *P. aeruginosa* strain unable to produce PVD and PCH, grew with the same efficiency in the absence or presence of 10 µM of **4,** indicating that bacteria were able to use this compound to access iron (Figure 7). However, growth in the presence of **4** was completely abolished upon deletion of the *pirA* gene, while the *pfeA* knock-out had no effect. This finding implies that **4** transported iron exclusively via PirA. In the presence of **6** or **7**, Δ*pvdF*Δ*pchA* growth was decreased by 63% and 82%, respectively, compared to the growth in the absence of any compounds. This indicated that **6** and **7** were not efficient in making iron accessible to *P. aeruginosa* cells, although the compounds were able to chelate iron (Figure 2). The residual growth observed with **6** appears to be PirA dependent, as the mutation of *pirA* gene abolished almost the growth completely. In conclusion, iron is transported by DOTAM **4** into *P. aeruginosa* cells via the TBDT PirA, but this uptake ability is affected by the presence of the payloads incorporated in **6** and **7**.

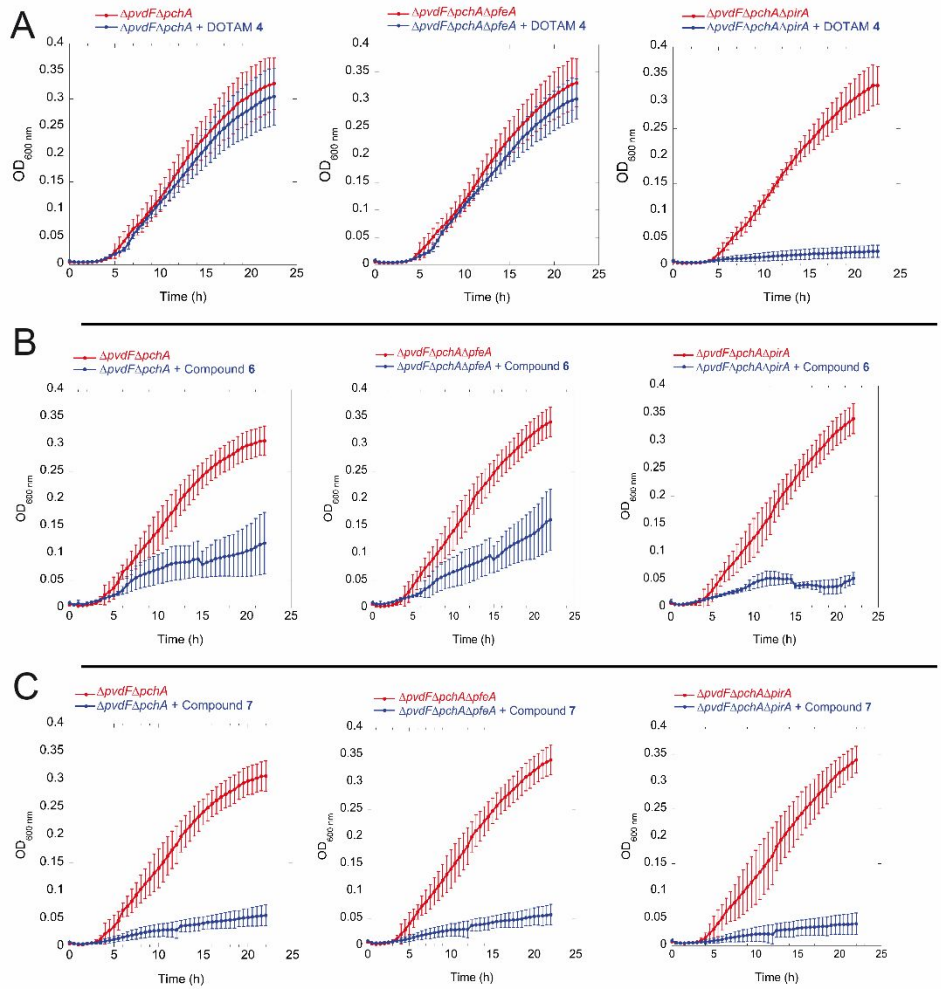

Figure 7. Growth of TBDT-deficient *P. aeruginosa* mutants in the presence of DOTAM-based siderophores 4, 6 and 7. A PVD and PCH-deficient strain of *P. aeruginosa* (Δ*pvdF*Δ*pchA*) and its corresponding TBDT deletion mutants were used. Strains were grown in CAA medium in the absence (kinetics in red) or presence (kinetics in blue) of 10 µM **4** (A), **6** (B) or **7** (C). Growth was followed by monitoring the optical density (OD) at 600 nm. Errors bars were calculated from three independent biological replicates.

DISCUSSION

Bacteria possess the ability to use artificial siderophores to access iron, and antibiotics can be linked to these compounds in order to enhance their transport across the bacterial membranes.[22,28–30] The use of synthetic siderophores and their antibiotic conjugates is possible, because bacteria often entertain a large panel of TBDTs involved in iron acquisition with different substrate specificities.[66–68]

P. aeruginosa has at least 20 genes encoding TBDTs involved in iron acquisition by siderophores and xenosiderophores.[17,69]

According to the present work, MECAM behaves in a similar way as ENT with respect to iron uptake in *P. aeruginosa* cells, except that MECAM seems to have a lower affinity for ferric ion chelation than ENT (Figure 2). In the literature, PfeA is considered as the major and PirA as a secondary TBDT for ferri-ENT.[42,54] Here, we observed that ferri-MECAM was mostly imported across the outer membrane by PfeA, but if this transporter was not expressed, PirA assumed the role very effectively (Figure 5). To date, the natural siderophore transported by PirA has not been identified, but it has been shown that PirA was able to import iron via catecholamines such as the neuromediators L-DOPA and norepinephrine.[58] The coupling of MECAM to ampicillin did not change its ability to chelate iron and transport it into *P. aeruginosa* cells *via* PfeA or PirA (Figures 4 and 5). However, PirA seems to be more relevant for the uptake of ferric **3** than for ferric **1**, suggesting that the presence of the antibiotic slightly affected the affinity of PfeA for **3** (Figure 4). Moreover, iron was effectively dissociated from **1** and **3**, as demonstrated by the growth of *P. aeruginosa* unable to produce its own siderophores PVD and PCH (Figure 5). If the iron remained chelated by MECAM in the bacteria, making it non-bioavailable, growth would be significantly affected.

The presence of **1-3** had several effects on the proteome of *P. aeruginosa*. First, the three compounds induced a strong expression of PfeA. This has also been reported previously by us for ENT, but also for another synthetic triscatechol siderophore, free or coupled with linezolid.[51,52] The fact that both the MECAM **1** and MECAM-ampicillin **3** induced the expression of the gene encoding their transporter PfeA is a clear advantage for the uptake of antibiotics by this transporter via a Trojan horse strategy, because the entrance route and hence the translocation of conjugates gets amplified. The conjugation to ampicillin did not affect the ability of MECAM to be translocated through the TBDTs PfeA and PirA and to interact with the sensor PfeS. In contrast, MECAM **1**/**2** and **3** were unable to interact with PirS and activate the transcription of *pirA*. The induction of PfeA expression went hand in hand with a repression of proteins involved in the PCH-dependent iron uptake pathway, suggesting that *P.*

aeruginosa cells will use MECAM **1** or MECAM-ampicillin **3** to acquire iron rather than its own siderophore PCH. However, the expression of the proteins of the PVD-dependent iron uptake pathway was not affected; in contrast, the presence of ENT in the same growth conditions repressed both the PCH and the PVD pathways.[17,51,52] and we assume that this is due to the higher iron affinity of ENT compared to the MECAM-based siderophores. Such phenotypic adaptation of *P. aeruginosa* cells to the presence of different xenosiderophores with different affinities for iron has already been described previously with ENT, vibriobactin, ferrichrome, nocardamine and yersiniabactin.[17,18] The observation that the effects on *P. aeruginosa* proteome obtained with MECAMs **1** and **2** were similar indicates that both compounds exert similar siderophore effects, and that the acetyl groups protecting the catechol groups in MECAM **2** were hydrolyzed in the bacterial growth media, as found for many other acetyl-protected catechols.[35,44] The presence of **3** in *P. aeruginosa* also induced the expression of *ampC*, which explains the absence of antibiotic activity for this conjugate. Thus, *P. aeruginosa* developed a resistance mechanism targeting the antibiotic and not at the expression level of the iron import pathways used by the vector. This illustrates that the vectorization of antibiotics by siderophores will not necessarily prevent the development of resistance against the antibiotic component.

All these data show that MECAM is a promising vector for the import of cargo into *P. aeruginosa* cells via the PfeA and PirA TBDTs. It should be kept in mind that ENT in *P. aeruginosa* cells is hydrolyzed in the bacterial periplasm and not in the cytoplasm, with this siderophore certainly never entering the cytoplasm;[70] also MECAM was shown to reach the periplasm, not the cytoplasm.[40] Consequently, to combat *P. aeruginosa*, it seems more promising to conjugate MECAM with antibiotics addressing targets in the periplasm. Along this line, a conjugate of MECAM to the relatively bulky cyclic lipopeptide daptomycin was recently prepared.[40] It showed promising activity against *A. baumannii*, but not against *P. aeruginosa*. Thus, it might be interesting to vectorize smaller, linear antimicrobial peptides affecting the integrity of the internal membrane by the MECAM core.

The DOTAM **4** has two metal binding sites, one triscatecholate site to chelate iron and the cyclen-based site, that has been used for chelating e.g. lanthanides, zinc[35] or radioactive gallium-68 for bacteria-specific PET imaging.[35,39] The competition experiment for iron with PVD showed that this vector had an affinity for iron that was comparable to MECAM. Proteomics data show that DOTAM-based siderophores **4, 5** and **7** chelated zinc very efficiently, as their presence induced an increase in the expression of two TBDTs involved in zinc acquisition, CntO and PA0781 (ZnuD). According to *P. aeruginosa* genome,[69] no transcriptional regulating sigma factors or two-component systems are associated to *cntO* and *PA0781* genes. Consequently the induction of the expression of these two zinc transporters is probably due to zinc starvation and involves the transcriptional regulator Zur[64,71] and not to the interaction of DOTAM with the sensor of some two-component system as shown above for MECAM. Compounds **4, 5** and **7** certainly chelate zinc in the environment of the bacteria, rendering bacterial cells zinc deficient. The upregulating effect was not observed with DOTAM-daptomycin **6**, suggesting that the presence of the antibiotic affects the ability of the DOTAM moiety to chelate zinc. According to the growth experiments with the strain unable to produce the endogenous siderophores PVD and PCH, DOTAM **4** imports iron into *P. aeruginosa* cells only through the TBDT PirA. PirA apparently recognizes substrates of relatively variable structures, since it imports ferric complexes with ENT, but also with catecholamines such as the neuromediators L-DOPA and norepinephrine.[58] The common motif is the coordination of iron by the catechols. Expression of *pirA* is inducible in the same way as *pfeA* by a two-component system, with PirS being the sensor and PirR the regulator (Figure S2). Since no induction of expression was observed in the presence of **4**/**5**, this molecule was probably not recognized by the sensor PirS. The presence of **4**/**5** in the environment of *P. aeruginosa* repressed the expression of proteins of the PCH pathway and had no effect on the PVD pathway, probably because the affinity for ferric iron of these compounds is higher than that of PCH and lower than that of PVD. This effect on the expression of the PCH pathway indicates that the bacteria used less PCH to access iron and favor the use of DOTAM molecules. Indeed, a previous study on the adaptation of the expression of the iron import pathways of *P. aeruginosa* grown in the presence of 10 µM ENT,

vibriobactin, ferrichrome, yersiniabactin, or nocardamine has demonstrated the importance of the tested siderophore's affinity for ferric iron on the expression levels of the corresponding uptake pathways [17,72]. *P. aeruginosa* adjusts the expression of its various iron-uptake pathways to match the competition for iron between the siderophores present.

While **4** could restore growth, the ability of **6** and **7** to import iron into *P. aeruginosa* cells was limited, as the PVD/PCH-deficient pathogen hardly grew in the presence of these compounds. Also the recognition of the molecules by PirA was affected, possibly due to their relative size. It remains interesting to test DOTAM conjugates with smaller payloads.

In conclusion, the present study provides insights how hexacoordinating artificial siderophores import iron and conjugated cargo into the Gram-negative pathogen *P. aeruginosa*. While such mimetics have advantages with respect to synthetic access and variability compared to natural siderophores, their functionality is often only assessed by global phenotypic experiments such as MIC assays, that reflect an overlay of multiple parameters. Here, we demonstrate iron stealing from endogenous siderophores, efficient iron transport into *P. aeruginosa*, identify the involved transporters and their regulation, and also show the limitations of these processes when the vectors carry a payload. All these data show that MECAM is a promising vector for antibiotic import into the periplasm of *P. aeruginosa*. From this point, a further structural optimization of the scaffolds, in combination with diverse linkers and antibiotics, is warranted to expand their utility as delivery vehicles.

MATERIALS AND METHODS

Chemical Methods. The protonophore carbonyl cyanide m-chlorophenylhydrazone (CCCP) was purchased from Sigma-Aldrich, and $^{55}FeCl_3$ was purchased from Perkin Elmer. Pyoverdine (PVD) was purified from *P. aeruginosa* PAO1 culture supernatants as described previously.[73] Enterobactin (ENT) and ferrichrome (FERRI) were purchased from Sigma-Aldrich. The MECAM siderophores **1, 2**, and **3** were synthetized as described previously.[40] DOTAM siderophores **4** and **5** were synthetized as

described in Ferreira et al[35] and conjugate **7** was synthetized as described in Peukert et al.[39] The synthesis of DOTAM conjugate **6** is described in the Supplemental Materials.

Bacterial strains and growth conditions. The *P. aeruginosa* PAO1 strains used in this study are listed in Table S3. For all experiments presented below, bacteria were first grown in LB medium overnight at 30°C, and then washed and resuspended in iron-deficient CAA (casamino acid) medium containing 5g l^{-1} low-iron CAA (Difco), 1.46 g l^{-1} K_2HPO_4 $3H_2O$ and 0.25 g l^{-1} $MgSO_4$ $7H_2O$ and grown overnight at 30°C. Afterwards, the bacteria were grown a second time overnight in CAA medium at 30°C in the presence of 10 µM of siderophores, vectors or conjugates if required for the experiment.

Iron scavenging from PVD-Fe. Compounds were prepared in stock solutions at 10 mM in DMSO (compounds **1**, **3**, **4**, **6** and **7**) or water (PVD, ENT and FERRI). PVD-Fe at 10 µM in 100 µL of HEPES buffer (100 mM, pH 7.4) was incubated at 25 °C for 48 h in the presence of increasing concentrations of ENT, FERRI, **1**, **3**, **4**, **6**, or **7**, and PVD fluorescence was monitored at 447 nm (excitation at 400 nm).[17] The data were normalized using the formula $(F_{MEASURED} - F_{PVD\text{-}Fe})/(F_{PVD} - F_{PVD\text{-}Fe})$, $F_{MEASURED}$ being the fluorescence measured for each experimental condition, $F_{PVD\text{-}Fe}$ the fluorescence of 10 µM PVD-Fe, and F_{PVD} the fluorescence of 10 µM PVD.

Label-free proteomics analysis. *P. aeruginosa* PAO1 cells grown in CAA medium were diluted to an $OD_{600\ nm}$ of 0.1 units and incubated in the absence or presence of 10 µM of **1**-**7** at 30°C for 8 h. $5x10^8$ cells from each culture were used for proteomic analysis. Each sample was prepared in biological triplicate for each cell culture condition. Cell pellets were resuspended in 200 µL of lysis buffer (UTCT buffer containing 7 M urea, 2 M thiourea, 4% CHAPS and 20 mM Tris-HCl pH 7.6) supplemented with nuclease and DNase. Protein concentrations were determined by a Bradford assay using bovine serum albumin as standard. Proteins were further precipitated overnight with glacial 0.1 M ammonium acetate in 100 % methanol (5 volumes, -20°C). After centrifugation at 12.000 g and 4°C during 15 min,

the resulting pellets were washed twice with 0.1 M ammonium acetate in 80% methanol and further dried under vacuum (Speed-Vac concentrator). Pellets were resuspended in 100 µL of 50 mM ammonium bicarbonate and submitted to reduction (5 mM dithiothreitol, 95°C, 10 min) and alkylation (10 mM iodoacetamide, room temperature, 20 min). Proteins were finally digested overnight with 150 ng of sequencing-grade trypsin (Promega). The proteomic datasets were obtained by the injection of 500 ng of each peptidic mixture on an orbitrap mass spectrometer (Q-Exactive Plus, Thermo-Fisher Scientific, USA) coupled to an EASY-nanoLC-1000 (Thermo-Fisher Scientific, USA) as described previously.[17]

The obtained raw data was converted to .mgf files with the Proteome Discoverer Daemon software (Thermo-Fisher Scientific, script "Export-to-mgf", version 2.2). For differential proteomic analyses, data was searched against the *P. aeruginosa* UniprotKB sub-database with a decoy strategy (UniprotKB release 2016_12, taxon 208964, *P. aeruginosa* strain PAO1, 5564 forward protein sequences). Peptides and proteins were identified with Mascot algorithm (version 2.5.1, Matrix Science, London, UK). The following parameters were used: (i) Trypsin/P was selected as enzyme, (ii) two missed cleavages were allowed, (iii) methionine oxidation and acetylation of protein N-term were set as variable modifications and carbamidomethylation of cysteine as fixed modification, (iv) mass tolerance for precursor ions was set at 10 ppm, and at 0.02 Da for fragment ions. Mascot data were further imported into Proline v1.4 software (http://proline.profiproteomics.fr/).[74] Proteins were validated on Mascot pretty rank equal to 1, and 1% FDR (False Discovery Rate) on both peptide spectrum matches (PSM score) and protein sets (Protein Set score). The total number of MS/MS fragmentation spectra was used to quantify each protein from at least three independent biological replicates: This "BasicSC" value calculated by Proline includes all PSMs of all peptides, including the modified peptides (three fixed and variable modifications) and the peptides shared by different protein sets. After a normalization of the data matrix with the total number of spectra in one sample, the "BasicSC" spectral count values were submitted to a negative-binomial test using an edgeR GLM regression through R (R v3.2.5). The statistical test was based on the published msmsTests R package available in Bioconductor to process

label-free LC-MS/MS data by spectral counts.[75] For each identified protein, an adjusted p-value (adjp) corrected by Benjamini–Hochberg was calculated, as well as a protein fold-change (FC). The MS data were deposited in the ProteomeXchange Consortium database via the PRIDE[76] partner repository with the dataset identifier: Project accession: PXD031065; Project DOI: 10.6019/PXD031065. Reviewer account details: **Username:** reviewer_pxd031065@ebi.ac.uk, **Password:** MX36hUWR.

Quantitative real-time PCR on bacteria grown in the presence of compounds 1-7. This RT-qPCR assay was carried out as described previously[17,51] on PAO1 cells grown in CAA medium the presence of 10 µM of compounds **1**-**7**. The primers used are listed in Table S4. An aliquot of 2.5 x 10^8 cells from this culture was added to two volumes of RNAprotect Bacteria Reagent (Qiagen) and exactly the same protocol was used as previously described.[17] Primer efficiency was determined using serially diluted genomic DNA and the double ΔC_T method was used to analyze qPCR data.

Iron uptake. Enterobactin-^{55}Fe, vectors-^{55}Fe and conjugates-^{55}Fe complexes were prepared at ^{55}Fe concentrations of 50 µM, with a compound:iron (mol:mol) ratio of 20:1 as described previously.[51] *P. aeruginosa* strains were successively grown an overnight in LB broth, followed by an overnight in CAA medium and at last an overnight in CAA medium with either 10 µM ENT, MECAM **1** or MECAM conjugate **3**. All these successive cultures were carried out at 30°C. The bacteria were subsequently used for ^{55}Fe uptake kinetics as described previously[51] in the absence and presence of 200 µM CCCP (a proton motive force inhibitor.[57]

Growth assays in iron-restricted conditions. For *P. aeruginosa* growth assays in microplates, bacteria were grown as described above: a first overnight culture at 30°C in 10 mL of LB broth, afterwards bacteria were washed and a second overnhight culture was carried out in 20 mL CAA medium at 30°C. Bacteria were then washed, resuspended in CAA medium at an optical density of 0.02 at 600 nm and distributed in the wells of a 96-well plate (Greiner, U-bottomed microplate) in the absence or presence

of 10 µM of compounds **1**, **3**, **4**, **6** and **7**. The plate was incubated at 30 °C, with shaking, in a TECAN microplate reader (Infinite M200, Tecan) and bacterial growth was monitored at $OD_{600\ nm}$. The presented data are the mean of three replicates for each measurement.

SUPPORTING INFORMATION

General chemical information; synthesis procedure of compounds **1**-**7**; table describing MIC values; table describing strains used in this study; table describing plasmids used in this study; 2 table describing primers used in this study; figure with the proteomic analyses in the presence of MECAM **2**; figure summarizing ENT-dependent iron uptake pathway in *P. aeruginosa*; figure showing RT-qPCR data with MECAM **1** and **3**; figures showing ^{55}Fe uptake and bacterial growth in the presence of bacillibactin; figure showing RT-qPCR data with DOTAM **4, 6** and **7;** figure with the proteomic analyses in the presence of DOTAM **5**.

CORRESPONDING AUTHOR INFORMATION

To whom correspondence should be addressed: isabelle.schalk@unistra.fr, mark.broenstrup@helmholtz-hzi.de

AUTHOR CONTRIBUTIONS

I.J., V.G. and M.B. conceived the idea and designed the experiments. C.P. and L.P. synthesized all the compounds synthetic siderophores and conjugates. S.F. performed bacterial cultures, ^{55}Fe uptake assays and iron competition with PVD, V.G. performed RT-qPCR assays. L.K. performed proteomic assays and L.K. and Q.P. proteome data analyzes. I.J.S, C.P and M.B. wrote the manuscript.

ABBREVIATIONS USED

DOTAM, tetrapodal 1,4,7,10-tetraazacyclododecane-1,4,7,10-tetraacetic amide; CAA, casamino acid; CCCP, Carbonyl cyanide-*m*-chlorophenylhydrazone; ENT, enterobactin ; PCH, pyochelin; PVD, pyoverdine; FERRI, ferrichrome; RT-qPCR , quantitative reverse transcription polymerase chain reaction; TBDT, TonB-dependent transporters.

ACKNOWLEDGMENTS

This work was partially funded by the *Centre National de la Recherche Scientifique*, a grant from the Joint Programming Initiative on Antimicrobial Resistance (JPI AMR, grant number: 01KI1825) and the Interdisciplinary Thematic Institute (ITI) InnoVec (Innovative Vectorization of Biomolecules, IdEx, ANR-10-IDEX-0002) and SFRI (ANR-20-SFRI-0012). The mass spectrometry instrumentation at the IBMC was funded by the University of Strasbourg, IdEx “Equipement mi-lourd” 2015. The equipment at the IPHC was partly funded by the French Proteomics Infrastructure (ProFI; ANR-10-INSB-08-03). QP had a fellowship from the associations Vaincre la Mucoviscidose and Gregory Lemarchal. CP had a Kekulé stipend from the ‘Verband der chemischen Industrie’, and LP was funded by the DFG project number BR 3572/4-1.

References

(1) Schalk, I. J.; Mislin, G. L. A.; Brillet, K. Structure, Function and Binding Selectivity and Stereoselectivity of Siderophore-Iron Outer Membrane Transporters. *Curr Top Membr* **2012**, *69*, 37–66. https://doi.org/10.1016/B978-0-12-394390-3.00002-1.

(2) Celia, H.; Noinaj, N.; Zakharov, S. D.; Bordignon, E.; Botos, I.; Santamaria, M.; Barnard, T. J.; Cramer, W. A.; Lloubes, R.; Buchanan, S. K. Structural Insight into the Role of the Ton Complex in Energy Transduction. *Nature* **2016**, *538* (7623), 60–65. https://doi.org/10.1038/nature19757.

(3) Celia, H.; Botos, I.; Ni, X.; Fox, T.; De Val, N.; Lloubes, R.; Jiang, J.; Buchanan, S. K. Cryo-

EM Structure of the Bacterial Ton Motor Subcomplex ExbB-ExbD Provides Information on Structure and Stoichiometry. *Commun Biol* **2019**, *2*, 358. https://doi.org/10.1038/s42003-019-0604-2.

(4) Moynié, L.; Milenkovic, S.; Mislin, G. L. A.; Gasser, V.; Malloci, G.; Baco, E.; McCaughan, R. P.; Page, M. G. P.; Schalk, I. J.; Ceccarelli, M.; Naismith, J. H. The Complex of Ferric-Enterobactin with Its Transporter from *Pseudomonas aeruginosa* Suggests a Two-Site Model. *Nat Commun* **2019**, *10* (1), 3673. https://doi.org/10.1038/s41467-019-11508-y.

(5) Josts, I.; Veith, K.; Tidow, H. Ternary Structure of the Outer Membrane Transporter FoxA with Resolved Signalling Domain Provides Insights into TonB-Mediated Siderophore Uptake. *eLife* **2019**, *8*, e48528. https://doi.org/10.7554/eLife.48528.

(6) Celia, H.; Noinaj, N.; Buchanan, S. K. Structure and Stoichiometry of the Ton Molecular Motor. *Int J Mol Sci* **2020**, *21* (2). https://doi.org/10.3390/ijms21020375.

(7) Schauer, K.; Gouget, B.; Carriere, M.; Labigne, A.; de Reuse, H. Novel Nickel Transport Mechanism across the Bacterial Outer Membrane Energized by the TonB/ExbB/ExbD Machinery. *Mol Microbiol* **2007**, *63* (4), 1054–1068.

(8) Schauer, K.; Rodionov, D. A.; de Reuse, H. New Substrates for TonB-Dependent Transport: Do We Only See the "Tip of the Iceberg"? *Trends Biochem Sci* **2008**, *33* (7), 330–338. https://doi.org/10.1016/j.tibs.2008.04.012.

(9) Lhospice, S.; Gomez, N. O.; Ouerdane, L.; Brutesco, C.; Ghssein, G.; Hajjar, C.; Liratni, A.; Wang, S.; Richaud, P.; Bleves, S.; Ball, G.; Borezée-Durant, E.; Lobinski, R.; Pignol, D.; Arnoux, P.; Voulhoux, R. *Pseudomonas aeruginosa* Zinc Uptake in Chelating Environment Is Primarily Mediated by the Metallophore Pseudopaline. *Sci Rep* **2017**, *7* (1), 17132. https://doi.org/10.1038/s41598-017-16765-9.

(10) Pieńko, T.; Czarnecki, J.; Równicki, M.; Wojciechowska, M.; Wierzba, A. J.; Gryko, D.;

Bartosik, D.; Trylska, J. Vitamin B12-Peptide Nucleic Acids Use the BtuB Receptor to Pass through the *Escherichia coli* Outer Membrane. *Biophys J* **2021**, *120* (4), 725–737. https://doi.org/10.1016/j.bpj.2021.01.004.

(11) Monge, E. C.; Gardner, J. G. Efficient Chito-Oligosaccharide Utilization Requires Two TonB-Dependent Transporters and One Hexosaminidase in *Cellvibrio japonicus*. *Mol Microbiol* **2021**, *116* (2), 366–380. https://doi.org/10.1111/mmi.14717.

(12) Hider, R. C.; Kong, X. Chemistry and Biology of Siderophores. *Nat Prod Rep* **2011**, *27* (5), 637–657. https://doi.org/10.1039/b906679a.

(13) Boukhalfa, H.; Crumbliss, A. L. Chemical Aspects Od Siderophore Mediated Iron Transport. *Biometals* **2002**, *15* (4), 325–339.

(14) Hider, R. Siderophore Mediated Absorption of Iron. *Struct Bonding* **1984**, *58*, 28.

(15) Loomis, L.; Raymond, K. N. Solution Equilibria of Enterobactin Complexes. *Inorg. Chem.* **1991**, *30*, 906–911.

(16) Galet, J.; Deveau, A.; Hôtel, L.; Frey-Klett, P.; Leblond, P.; Aigle, B. *Pseudomonas fluorescens* Pirates Both Ferrioxamine and Ferricoelichelin Siderophores from *Streptomyces ambofaciens*. *Appl. Environ. Microbiol.* **2015**, *81* (9), 3132–3141. https://doi.org/10.1128/AEM.03520-14.

(17) Perraud, Q.; Cantero, P.; Roche, B.; Gasser, V.; Normant, V. P.; Kuhn, L.; Hammann, P.; Mislin, G. L. A.; Ehret-Sabatier, L.; Schalk, I. J. Phenotypic Adaption of *Pseudomonas aeruginosa* by Hacking Siderophores Produced by Other Microorganisms. *Mol. Cell Proteomics* **2020**, *19* (4), 589–607. https://doi.org/10.1074/mcp.RA119.001829.

(18) Normant, V.; Josts, I.; Kuhn, L.; Perraud, Q.; Fritsch, S.; Hammann, P.; Mislin, G. L. A.; Tidow, H.; Schalk, I. J. Nocardamine-Dependent Iron Uptake in *Pseudomonas aeruginosa:* Exclusive Involvement of the FoxA Outer Membrane Transporter. *ACS Chem. Biol.* **2020**.

15(10):2741-2751. https://doi.org/10.1021/acschembio.0c00535.

(19) Schalk, I. J.; Rigouin, C.; Godet, J. An Overview of Siderophore Biosynthesis among Fluorescent Pseudomonads and New Insights into Their Complex Cellular Organization. *Environ. Microbiol.* **2020**, *22* (4), 1447–1466. https://doi.org/10.1111/1462-2920.14937.

(20) Llamas, M. A.; Mooij, M. J.; Sparrius, M.; Vandenbroucke-Grauls, C. M.; Ratledge, C.; Bitter, W. Characterization of Five Novel *Pseudomonas aeruginosa* Cell-Surface Signalling Systems. *Mol Microbiol* **2008**, *67* (2), 458–472.

(21) Hannauer, M.; Barda, Y.; Mislin, G. L.; Shanzer, A.; Schalk, I. J. The Ferrichrome Uptake Pathway in *Pseudomonas aeruginosa* Involves an Iron Release Mechansim with Acylation of the Siderophore and a Recycling of the Modified Desferrichrome. *J Bacteriol* **2010**, *192*, 1212–1220. https://doi.org/10.1128/JB.01539-09.

(22) Mislin, G. L. A.; Schalk, I. J. Siderophore-Dependent Iron Uptake Systems as Gates for Antibiotic Trojan Horse Strategies against *Pseudomonas aeruginosa*. *Metallomics* **2014**, *6* (3), 408–420. https://doi.org/10.1039/c3mt00359k.

(23) Schalk, I. J.; Mislin, G. L. A. Bacterial Iron Uptake Pathways: Gates for the Import of Bactericide Compounds. *J. Med. Chem.* **2017**, *60* (11), 4573–4576. https://doi.org/10.1021/acs.jmedchem.7b00554.

(24) Schalk, I. J. Siderophore-Antibiotic Conjugates: Exploiting Iron Uptake to Deliver Drugs into Bacteria. *Clin. Microbiol. Infect.* **2018**, *24* (8), 801–802. https://doi.org/10.1016/j.cmi.2018.03.037.

(25) Negash, K. H.; Norris, J. K. S.; Hodgkinson, J. T. Siderophore-Antibiotic Conjugate Design: New Drugs for Bad Bugs? *Molecules* **2019**, *24* (18), E3314. https://doi.org/10.3390/molecules24183314.

(26) Zheng, T.; Bullock, J. L.; Nolan, E. M. Siderophore-Mediated Cargo Delivery to the

Cytoplasm of *Escherichia coli* and *Pseudomonas aeruginosa*: Syntheses of Monofunctionalized Enterobactin Scaffolds and Evaluation of Enterobactin-Cargo Conjugate Uptake. *J Am Chem Soc* **2012**, *134* (44), 18388–18400. https://doi.org/10.1021/ja3077268.

(27) Zheng, T.; Nolan, E. M. Enterobactin-Mediated Delivery of Beta-Lactam Antibiotics Enhances Antibacterial Activity against Pathogenic *Escherichia coli*. *J Am Chem Soc* **2014**, *136* (27), 9677–9691. https://doi.org/10.1021/ja503911p.

(28) Górska, A.; Sloderbach, A.; Marszałł, M. P. Siderophore-Drug Complexes: Potential Medicinal Applications of the "Trojan Horse" Strategy. *Trends Pharmacol. Sci.* **2014**, *35* (9), 442–449. https://doi.org/10.1016/j.tips.2014.06.007.

(29) Miller, M. J.; Liu, R. Design and Syntheses of New Antibiotics Inspired by Nature's Quest for Iron in an Oxidative Climate. *Acc. Chem. Res.* **2021**, *54* (7), 1646–1661. https://doi.org/10.1021/acs.accounts.1c00004.

(30) Sargun, A.; Gerner, R. R.; Raffatellu, M.; Nolan, E. M. Harnessing Iron Acquisition Machinery to Target Enterobacteriaceae. *J Infect Dis* **2021**, *223* (12 Suppl 2), S307–S313. https://doi.org/10.1093/infdis/jiaa440.

(31) Choi, J. J.; McCarthy, M. W. Cefiderocol: A Novel Siderophore Cephalosporin. *Expert Opin Investig Drugs* **2018**, *27* (2), 193–197. https://doi.org/10.1080/13543784.2018.1426745.

(32) Silva, J. T.; López-Medrano, F. Cefiderocol, a New Antibiotic against Multidrug-Resistant Gram-Negative Bacteria. *Rev Esp Quimioter* **2021**, *34 Suppl 1*, 41–43. https://doi.org/10.37201/req/s01.12.2021.

(33) Syed, Y. Y. Cefiderocol: A Review in Serious Gram-Negative Bacterial Infections. *Drugs* **2021**, *81* (13), 1559–1571. https://doi.org/10.1007/s40265-021-01580-4.

(34) Auletta, S.; Galli, F.; Lauri, C.; Martinelli, D.; Santino, I.; Signore, A. Imaging Bacteria with Radiolabelled Quinolones, Cephalosporins and Siderophores for Imaging Infection: A

Systematic Review. *Clin Transl Imaging* **2016**, *4*, 229–252. https://doi.org/10.1007/s40336-016-0185-8.

(35) Ferreira, K.; Hu, H.-Y.; Fetz, V.; Prochnow, H.; Rais, B.; Müller, P. P.; Brönstrup, M. Multivalent Siderophore-DOTAM Conjugates as Theranostics for Imaging and Treatment of Bacterial Infections. *Angew. Chem. Int. Ed. Engl.* **2017**, *56* (28), 8272–8276. https://doi.org/10.1002/anie.201701358.

(36) Dutta, J.; Naicker, T.; Ebenhan, T.; Kruger, H. G.; Arvidsson, P. I.; Govender, T. Synthetic Approaches to Radiochemical Probes for Imaging of Bacterial Infections. *Eur J Med Chem* **2017**, *133*, 287–308. https://doi.org/10.1016/j.ejmech.2017.03.060.

(37) Petrik, M.; Pfister, J.; Misslinger, M.; Decristoforo, C.; Haas, H. Siderophore-Based Molecular Imaging of Fungal and Bacterial Infections-Current Status and Future Perspectives. *J Fungi (Basel)* **2020**, *6* (2), E73. https://doi.org/10.3390/jof6020073.

(38) Petrik, M.; Umlaufova, E.; Raclavsky, V.; Palyzova, A.; Havlicek, V.; Pfister, J.; Mair, C.; Novy, Z.; Popper, M.; Hajduch, M.; Decristoforo, C. 68Ga-Labelled Desferrioxamine-B for Bacterial Infection Imaging. *Eur J Nucl Med Mol Imaging* **2021**, *48* (2), 372–382. https://doi.org/10.1007/s00259-020-04948-y.

(39) Peukert, C.; Langer, L. N. B.; Wegener, S. M.; Tutov, A.; Bankstahl, J. P.; Karge, B.; Bengel, F. M.; Ross, T. L.; Brönstrup, M. Optimization of Artificial Siderophores as 68Ga-Complexed PET Tracers for *in vivo* Imaging of Bacterial Infections. *J. Med. Chem.* **2021**, *64* (16), 12359–12378. https://doi.org/10.1021/acs.jmedchem.1c01054.

(40) Pinkert, L.; Lai, Y.-H.; Peukert, C.; Hotop, S.-K.; Karge, B.; Schulze, L. M.; Grunenberg, J.; Brönstrup, M. Antibiotic Conjugates with an Artificial MECAM-Based Siderophore Are Potent Agents against Gram-Positive and Gram-Negative Bacterial Pathogens. *J Med Chem* **2021**, *64* (20), 15440–15460. https://doi.org/10.1021/acs.jmedchem.1c01482.

(41) Dean, C. R.; Poole, K. Cloning and Characterization of the Ferric Enterobactin Receptor Gene (*pfeA*) of *Pseudomonas aeruginosa*. *J. Bacteriol.* **1993**, *175* (2), 317–324.

(42) Gasser, V.; Kuhn, L.; Hubert, T.; Aussel, L.; Hammann, P.; Schalk, I. J. The Esterase PfeE, the Achilles' Heel in the Battle for Iron between *Pseudomonas aeruginosa* and *Escherichia coli*. *Int J Mol Sci* **2021**, *22* (6), 2814. https://doi.org/10.3390/ijms22062814.

(43) Livermore, D. M. Multiple Mechanisms of Antimicrobial Resistance in *Pseudomonas aeruginosa*: Our Worst Nightmare? *Clin Infect Dis* **2002**, *34* (5), 634–640. https://doi.org/10.1086/338782.

(44) Ohi, N.; Aoki, B.; Kuroki, T.; Matsumoto, M.; Kojima, K.; Nehashi, T. Semisynthetic Beta-Lactam Antibiotics. III. Effect on Antibacterial Activity and Comt-Susceptibility of Chlorine-Introduction into the Catechol Nucleus of 6-[(R)-2-[3-(3,4-Dihydroxybenzoyl)-3-(3-Hydroxypropyl)-1-Ureido]-2- Phenylacetamido]Penicillanic Acid. *J Antibiot (Tokyo)* **1987**, *40* (1), 22–28. https://doi.org/10.7164/antibiotics.40.22.

(45) Albrecht-Gary, A. M.; Blanc, S.; Rochel, N.; Ocacktan, A. Z.; Abdallah, M. A. Bacterial Iron Transport: Coordination Properties of Pyoverdin PaA, a Peptidic Siderophore of *Pseudomonas aeruginosa*. *Inorg. Chem.* **1994**, *33*, 6391–6402.

(46) Folschweiller, N.; Gallay, J.; Vincent, M.; Abdallah, M. A.; Pattus, F.; Schalk, I. J. The Interaction between Pyoverdin and Its Outer Membrane Receptor in *Pseudomonas aeruginosa* Leads to Different Conformers: A Time-Resolved Fluorescence Study. *Biochemistry* **2002**, *41* (49), 14591–14601.

(47) Brandel, J.; Humbert, N.; Elhabiri, M.; Schalk, I. J.; Mislin, G. L. A.; Albrecht-Garry, A.-M. Pyochelin, a Siderophore of *Pseudomonas aeruginosa*: Physicochemical Characterization of the Iron(III), Copper(II) and Zinc(II) Complexes. *Dalton Trans* **2012**, *41* (9), 2820–2834.

(48) Anderegg, G.; L'Eplattenier, F.; Schwarzenbach, G. Hydroxamatkomplexe III. Eisen(III)-

Austausch Zwischen Sideraminen Und Komplexonen. Diskussion Der Bildungskonstanten Der Hydroxamatkomplexe. *Helvetica Chimica Acta* **1963**, *46* (4), 1409–1422. https://doi.org/10.1002/hlca.19630460436.

(49) Llamas, M. A.; Sparrius, M.; Kloet, R.; Jimenez, C. R.; Vandenbroucke-Grauls, C.; Bitter, W. The Heterologous Siderophores Ferrioxamine B and Ferrichrome Activate Signaling Pathways in *Pseudomonas aeruginosa*. *J Bacteriol* **2006**, *188* (5), 1882–1891.

(50) Llamas, M. A.; Imperi, F.; Visca, P.; Lamont, I. L. Cell-Surface Signaling in Pseudomonas: Stress Responses, Iron Transport, and Pathogenicity. *FEMS Microbiol Rev* **2014**, *38* (4), 569–597. https://doi.org/10.1111/1574-6976.12078.

(51) Gasser, V.; Baco, E.; Cunrath, O.; August, P. S.; Perraud, Q.; Zill, N.; Schleberger, C.; Schmidt, A.; Paulen, A.; Bumann, D.; Mislin, G. L. A.; Schalk, I. J. Catechol Siderophores Repress the Pyochelin Pathway and Activate the Enterobactin Pathway in *Pseudomonas aeruginosa*: An Opportunity for Siderophore-Antibiotic Conjugates Development. *Environ. Microbiol.* **2016**, *18* (3), 819–832. https://doi.org/10.1111/1462-2920.13199.

(52) Perraud, Q.; Cantero, P.; Munier, M.; Hoegy, F.; Zill, N.; Gasser, V.; Mislin, G. L. A.; Ehret-Sabatier, L.; Schalk, I. J. Phenotypic Adaptation of *Pseudomonas aeruginosa* in the Presence of Siderophore-Antibiotic Conjugates during Epithelial Cell Infection. *Microorganisms* **2020**, *8* (11). https://doi.org/10.3390/microorganisms8111820.

(53) Cunrath, O.; Geoffroy, V. A.; Schalk, I. J. Metallome of *Pseudomonas aeruginosa*: A Role for Siderophores. *Environ. Microbiol.* **2016**, *18* (10), 3258–3267. https://doi.org/10.1111/1462-2920.12971.

(54) Ghysels, B.; Ochsner, U.; Mollman, U.; Heinisch, L.; Vasil, M.; Cornelis, P.; Matthijs, S. The *Pseudomonas aeruginosa pirA* Gene Encodes a Second Receptor for Ferrienterobactin and Synthetic Catecholate Analogues. *FEMS Microbiol Lett* **2005**, *246* (2), 167–174.

(55) Dean, C. R.; Poole, K. Expression of the Ferric Enterobactin Receptor (PfeA) of *Pseudomonas aeruginosa*: Involvement of a Two-Component Regulatory System. *Mol Microbiol* **1993**, *8* (6), 1095–1103.

(56) Moynié, L.; Luscher, A.; Rolo, D.; Pletzer, D.; Tortajada, A.; Weingart, H.; Braun, Y.; Page, M. G. P.; Naismith, J. H.; Köhler, T. Structure and Function of the PiuA and PirA Siderophore-Drug Receptors from *Pseudomonas aeruginosa* and *Acinetobacter baumannii*. *Antimicrob. Agents Chemother.* **2017**, *61* (4). https://doi.org/10.1128/AAC.02531-16.

(57) Clément, E.; Mesini, P. J.; Pattus, F.; Abdallah, M. A.; Schalk, I. J. The Binding Mechanism of Pyoverdin with the Outer Membrane Receptor FpvA in *Pseudomonas aeruginosa* Is Dependent on Its Iron-Loaded Status. *Biochemistry* **2004**, *43*, 7954–7965.

(58) Perraud, Q.; Kuhn, L.; Fritsch, S.; Graulier, G.; Gasser, V.; Normant, V.; Hammann, P.; Schalk, I. J. Opportunistic Use of Catecholamine Neurotransmitters as Siderophores to Access Iron by *Pseudomonas aeruginosa*. *Environ Microbiol* **2020**. https://doi.org/10.1111/1462-2920.15372.

(59) Cox, C. D. Iron Uptake with Ferripyochelin and Ferriccitrate by *Pseudomonas aeruginosa*. *J Bacteriol* **1980**, *142*, 581–587.

(60) Marshall, B.; Stintzi, A.; Gilmour, C.; Meyer, J.-M.; Poole, K. Citrate-Mediated Iron Uptake in *Pseudomonas aeruginosa*: Involvement of the Citrate-Inducible FecA Receptor and the FeoB Ferrous Iron Transporter. *Microbiology (Reading, Engl.)* **2009**, *155* (Pt 1), 305–315. https://doi.org/10.1099/mic.0.023531-0.

(61) Seyedmohammad, S.; Fuentealba, N. A.; Marriott, R. A. J.; Goetze, T. A.; Edwardson, J. M.; Barrera, N. P.; Venter, H. Structural Model of FeoB, the Iron Transporter from *Pseudomonas aeruginosa*, Predicts a Cysteine Lined, GTP-Gated Pore. *Biosci Rep* **2016**, *36* (2), e00322. https://doi.org/10.1042/BSR20160046.

(62) McFarlane, J. S.; Lamb, A. L. Biosynthesis of an Opine Metallophore by *Pseudomonas aeruginosa*. *Biochemistry* **2017**, *56* (45), 5967–5971. https://doi.org/10.1021/acs.biochem.7b00804.

(63) Hermansen, G. M. M.; Hansen, M. L.; Khademi, S. M. H.; Jelsbak, L. Intergenic Evolution during Host Adaptation Increases Expression of the Metallophore Pseudopaline in *Pseudomonas aeruginosa*. *Microbiology* **2018**, *164* (8), 1038–1047. https://doi.org/10.1099/mic.0.000687.

(64) Pederick, V. G.; Eijkelkamp, B. A.; Begg, S. L.; Ween, M. P.; McAllister, L. J.; Paton, J. C.; McDevitt, C. A. ZnuA and Zinc Homeostasis in *Pseudomonas aeruginosa*. *Sci Rep* **2015**, *5*, 13139. https://doi.org/10.1038/srep13139.

(65) Calmettes, C.; Ing, C.; Buckwalter, C. M.; El Bakkouri, M.; Chieh-Lin Lai, C.; Pogoutse, A.; Gray-Owen, S. D.; Pomès, R.; Moraes, T. F. The Molecular Mechanism of Zinc Acquisition by the Neisserial Outer-Membrane Transporter ZnuD. *Nat Commun* **2015**, *6* (1), 7996. https://doi.org/10.1038/ncomms8996.

(66) Kingsley, R.; Rabsch, W.; Stephens, P.; Roberts, M.; Reissbrodt, R.; Williams, P. H. Iron Supplying Systems of Salmonella in Diagnostics, Epidemiology and Infection. *FEMS Immunol Med Microbiol* **1995**, *11* (4), 257–264. https://doi.org/10.1111/j.1574-695X.1995.tb00154.x.

(67) Braun, V. Iron Uptake by *Escherichia coli*. *Front Biosci* **2003**, *8*, 1409–1421.

(68) Cornelis, P.; Dingemans, J. *Pseudomonas aeruginosa* Adapts Its Iron Uptake Strategies in Function of the Type of Infections. *Front Cell Infect Microbiol* **2013**, *3*, 75. https://doi.org/10.3389/fcimb.2013.00075.

(69) Winsor, G. L.; Griffiths, E. J.; Lo, R.; Dhillon, B. K.; Shay, J. A.; Brinkman, F. S. L. Enhanced Annotations and Features for Comparing Thousands of Pseudomonas Genomes in the Pseudomonas Genome Database. *Nucleic Acids Res.* **2016**, *44* (D1), D646-653.

https://doi.org/10.1093/nar/gkv1227.

(70) Perraud, Q.; Moynié, L.; Gasser, V.; Munier, M.; Godet, J.; Hoegy, F.; Mély, Y.; Mislin, G. L. A.; Naismith, J. H.; Schalk, I. J. A Key Role for the Periplasmic PfeE Esterase in Iron Acquisition via the Siderophore Enterobactin in *Pseudomonas aeruginosa*. *ACS Chem. Biol.* **2018**, *13* (9), 2603–2614. https://doi.org/10.1021/acschembio.8b00543.

(71) Outten, C. E.; Tobin, D. A.; Penner-Hahn, J. E.; O'Halloran, T. V. Characterization of the Metal Receptor Sites in *Escherichia coli Zur*, an Ultrasensitive Zinc(II) Metalloregulatory Protein. *Biochemistry* **2001**, *40* (35), 10417–10423.

(72) Normant, V.; Josts, I.; Kuhn, L.; Perraud, Q.; Fritsch, S.; Hammann, P.; Mislin, G. L. A.; Tidow, H.; Schalk, I. J. Nocardamine-Dependent Iron Uptake in *Pseudomonas aeruginosa*: Exclusive Involvement of the FoxA Outer Membrane Transporter. *ACS Chem. Biol.* **2020**, *15* (10), 2741–2751. https://doi.org/10.1021/acschembio.0c00535.

(73) Demange, P.; Bateman, A.; Mertz, C.; Dell, A.; Piémont, Y.; Abdallah, M. A. Bacterial Siderophores: Structures of Pyoverdins Pt, Siderophores of *Pseudomonas tolaasii* NCPPB 2192, and Pyoverdins Pf, Siderophores of *Pseudomonas fluorescens* CCM 2798. Identification of an Unusual Natural Amino Acid. *Biochemistry* **1990**, *29* (50), 11041–11051. https://doi.org/10.1021/bi00502a005.

(74) Bouyssié, D.; Hesse, A.-M.; Mouton-Barbosa, E.; Rompais, M.; Macron, C.; Carapito, C.; Gonzalez de Peredo, A.; Couté, Y.; Dupierris, V.; Burel, A.; Menetrey, J.-P.; Kalaitzakis, A.; Poisat, J.; Romdhani, A.; Burlet-Schiltz, O.; Cianférani, S.; Garin, J.; Bruley, C. Proline: An Efficient and User-Friendly Software Suite for Large-Scale Proteomics. *Bioinformatics* **2020**, *36* (10), 3148–3155. https://doi.org/10.1093/bioinformatics/btaa118.

(75) Gregori, J.; Sanchez, A.; Villanueva, J. *MsmsTests: LC-MS/MS Differential Expression Tests*; Bioconductor version: Release (3.9), 2019.

https://doi.org/10.18129/B9.bioc.msmsTests.

(76) Vizcaíno, J. A.; Csordas, A.; del-Toro, N.; Dianes, J. A.; Griss, J.; Lavidas, I.; Mayer, G.; Perez-Riverol, Y.; Reisinger, F.; Ternent, T.; Xu, Q.-W.; Wang, R.; Hermjakob, H. 2016 Update of the PRIDE Database and Its Related Tools. *Nucleic Acids Res.* **2016**, *44* (D1), D447-456. https://doi.org/10.1093/nar/gkv1145.

For Table of Contents Use Only

Uptake mechanisms and regulatory responses to MECAM- and DOTAM-based artificial siderophores and their antibiotic conjugates in *Pseudomonas aeruginosa*

Sarah Fritsch[1,2], Véronique Gasser[1,2], Carsten Peukert[4], Lukas Pinkert[4], Lauriane Kuhn[3], Quentin Perraud[1,2], , Vincent Normant[1,2], Mark Brönstrup[4,5,6*] and Isabelle J. Schalk[1,2 *].

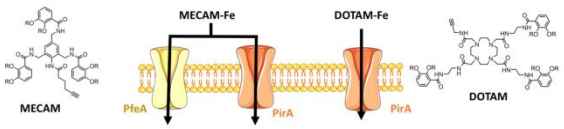

Fe uptake in *P. aeruginosa* by MECAM and DOTAM

The graphic show the two mimetics siderophores MECAM (1,3,5-N,N',N"-tris-(2,3-dihydroxybenzoyl)-triaminomethylbenzene) and DOTAM (1,4,7,10-Tetrakis(carbamoylmethyl)-1,4,7,10-tetraazacyclododecane), both chelating iron via catechol groups. These compounds have been recently applied as versatile carriers of functional antibiotics. In the present work, we have shown that MECAM imports iron into *P. aeruginosa* cells via the outer membrane transporters PfeA and PirA and DOTAM only by PirA.